Enhanced Wetland Classification using Deep Learning based Fusion Approach on Multi-Source Remote Sensing Images

Bahromjon Urmanov[1,*], Maha Ibrahim[1]

[1]Tashkent State University of economics, Tashkent, Uzbekistan

Emails: urmanov1983@gmail.com, M.Abdelazeem@tsue.uz

Abstract

Accurate remote sensing (RS) monitoring of wetland ground objects is an enormous importance for ecological preservation. Wetland classification on multi-source remote sensing images (MS-RSI) includes leveraging data from different sensors for accurately describing and categorizing wetland regions. This method normally incorporates data from infrared, radar, and optical sensors to take a wide-ranging view of wetland features. Advanced image processing methodologies, comprising machine learning (ML) approaches are often implemented for analyzing these multi-source images as well as recognizing spectral and spatial patterns indicative of wetland characteristics. The interaction of various RS data increases the accuracy and robustness of wetland classification models, allowing a more complex analysis of wetland ecosystems and aiding environmental observation, conservation, and control measures. To accomplish effective training for wetland mapping through the RS, it is essential for a significant training data that comprises a numerous array of class variants. In this article, we propose an Enhanced Wetland Classification using a Deep Learning based Fusion Approach (EWC-DLFA) on MS-RSI. The proposed EWC-DLFA technique examines the MS-RSI for wetland classification using the DL model which can be used for other land cover classification types. To accomplish this, the EWC-DLFA technique utilizes the data from multiple sources such as Sentinel-1 (SAR), Landsat-8, Sentinel2 (multi-spectral), and digital elevation model (DEM). In the presented EWC-DLFA technique, a deep convolutional neural network-based EfficientNetB-5 model can be applied for the extraction of features from the multi-source images. For increasing the performance of the EfficientNet-B5 model, the marine predators algorithm (MPA) based hyper parameter tuning process can be applied. Finally, an ensemble of three ML classifiers such as extreme learning machine (ELM), multilayer perceptron (MLP), and gradient boosting machine (GBM) are used to classify the wetland into different types such as fen, bog, marsh, swamps, and upland. The performance of the EWC-DLFA technique can be validated using a large set of simulations. The resultant values pointed out that the EWC-DLFA technique reaches better performance over other models on wetland classification.

Keywords: Wetland; Remote Sensing; Deep Learning; Marine Predators Algorithm; Fusion Model

1. Introduction

Wetlands are ecosystems that have been constantly or provisionally saturated or flooded with water; it helps soil structures, vegetation communities, and even species of wild animals, which increases in these situations [1]. Wetlands provide several advantages to society. The ecosystems offer a habitation for a diversity of flora and fauna and production in farming. Furthermore, they provide essential purposes namely the avoidance of flooding, protection of water quality, and controlling wastewater treatment and disposal [2]. Consequently, the preservation and safety of wetlands have become important to safeguard a viable future for both humans and their surroundings, as they perform an important function in the worldwide climatic cycle. Remote sensing (RS) offers numerous sources of data, every with its benefits [3]. Optical RS could be employed for evaluating functional features like chlorophyll and leaf moisture content. Synthetic aperture radar (SAR) data is implemented for determining

DOI: https://doi.org/10.54216/IJAACI.060102
Received: October 29, 2023 Revised: January 20, 2023 Accepted: June 10, 2024

biomass, moisture content, roughness, and geometric properties, particularly over huge regions [4]. Digital elevation models (DEMs) perform a vital function in wetland classification techniques with the help of major inputs, which allow the limit of wetland incidence dependent upon grade as well as other topographical features [5]. Meteorological information sources (for example, precipitation data) will also increase accuracy as it is employed to model temporal implications to be provided for wetness. Multiple source RS gives additional data that has a significant to fix limitations as well as enhance the possibility of wetland classification [6].

The fusion of multi-source data offers an innovative method for large-scale wetland classification, however, it is still a few issues that could be resolved: initially, it is complex to synthesize precise time series images of the coverage in the regional scale because of the limits of cloud and satellite revisit times [7]. The current study on multi-source image fusion frequently produces and combines images within the time window under the mean or media or fills in the gaps with images at nearby periods that could be caused by local variances because of unpredictable observational time and annotations. Additionally, the images acquired by these combinations are not original observation data, and the original data from numerous single-temporal images in the research field is lost [8]. Moreover, several researchers tend to utilize the easy and direct layer stacking technique for the SAR band and optical band. With the developments in time-series images and spectral features, the feature parameters of the model input quickly improve to multiple that not only creates the function complexity as well as decreases the processing speed but in the condition of restricted instances, excessive features could be caused the minimization of classification accuracy that is known as “dimension disaster”. Prior research implemented machine learning (ML) algorithms like Random Forest (RF), Support Vector Machine (SVM), and Decision Tree (DT) for recognizing wetlands that depend on multi-temporal observations [9]. While ML techniques enhance classification effectiveness by improving dimensions of input variables as well as diminishing the necessity for describing threshold-based classification approaches, the temporal relationship in multi-temporal satellite data is not entirely utilized and automatically employed [10]. In recent times, research revealed that a series of deep learning (DL) methods could effectively examine the sequential relationships within time-series RS data for wetland classification.

This article proposes an Enhanced Wetland Classification using Deep Learning based Fusion Approach (EWC-DLFA) on MS-RSI. In the presented EWC-DLFA technique, deep convolutional neural network-based EfficientNetB-5 model can be applied for the extraction of features from the multi-source images. For increasing the performance of the EfficientNet-B5 model, the marine predators algorithm (MPA) based hyper parameter tuning process can be applied. Finally, an ensemble of three ML classifiers such as multilayer perceptron (MLP), extreme learning machine (ELM), and gradient boosting machine (GBM) are used to classify the wetland into different types such as fen, bog, marsh, swamps, and upland. The resultant values pointed out that the EWC-DLFA technique reaches better performance over other models on wetland classification.

2. Related works

In [11], a 3D-UNet Generative Adversarial Network Swine Transformer (3D-UNet-GSFormer) method was developed for adjustably making the wetland training that depends on all types of data accessibility. Both synthesized and real training data have been further introduced to a new DL method that includes vision transformers and cutting-edge CNNs for wetland mapping. Hosseiny et al. [12] planned to design a classification model for mapping intricate wetland regions by integrating ensemble DL and satellite databases. The time series of the Sentinel-1 (S1) dual-polarized-SAR database, together with Sentinel-2 (S2) multi-spectral images (MSI), can be implemented as input data for the model. The developed WetNet model includes 3 various sub-models and numerous convolutional and recurrent layers. Besides, several ensemble units were included for diverse phases of the model.

In [13], an unsupervised multi-domain feature fusion and supervised classification network (UF2SCN) was developed. Primarily, an unsupervised single branch end-wise network was built for obtaining LiDAR and HSI fusion features. Secondarily, a supervised classification model with spatial attention has been implemented for employing fusion feature in categorization that applies the confined instances. Lastly, a 2 phases training approach was developed for increasing the capability of feature fusion. In [14], a DL fusion model that efficiently employs NDVI named the Dense-Spectral-Location-NDVI network (DSLN) method was developed. This method initially removes spatial location data in NDVI data simultaneously with RSI data. Next, the spectral feature was fed into the encoding-decoding configuration for extracting the depth features as well as renovating the spatial data. The NDVI fusion model was implemented for the combination of the depth features and NDVI data.

DOI: https://doi.org/10.54216/IJAACI.060102
Received: October 29, 2023 Revised: January 20, 2023 Accepted: June 10, 2024

Bosco et al. [15] presented a multi-granularity-NN Encoding model dependent upon VGG16, InceptionReseNet-V2, DenseNet201, and Inception-V3 frameworks into RSI classification. By applying pre-trained CNNs, ensemble learning and activation functions have been employed. InceptionV3 and VGG16 were implemented for extracting features. InceptionResNetV2 was applied for fine-tuning including releasing the whole model as well as retraining the novel data with a lesser learning rate. Hu et al. [16] examined and implemented 2 artificial neural networks (ANNs) based ensemble methods like Multi-boost-ANN (MB-ANN) and rotation-ANN (RANN) architecture. The RANN trains and integrates different ANNs by making a series of sparse rotation matrices, while the MBANN has been designed from sequential repetition in incorporation with the parallel sampling approach. The VGG11 and RF could be employed for contrast with these algorithms.

Yan et al. [17] projected a semantic segmentation network that integrates optical and radar SITS called the multi-source temporal attention (TA) fusion-enabled temporal-spatial transformer (MTAF-TST) method. Initially, the transformer spatial semantic segmentation model is implemented for extraction. Then, the transformer period feature extraction method is performed. Lastly, a multiple-source TA fusion component is implemented. Jafarzadeh et al. [18] proposed a multi-modal DL method dependent upon the incorporation of the graph convolutional network (GCN) and shallow CNN. Now, moderate-resolution S1-SAR and S2-MSI have been provided in the CNN and GCN techniques. The cooperation of S1 SAR and S2 optical images could be employed for removing diverse categories of wetland features as well as improving the probability of class discrimination.

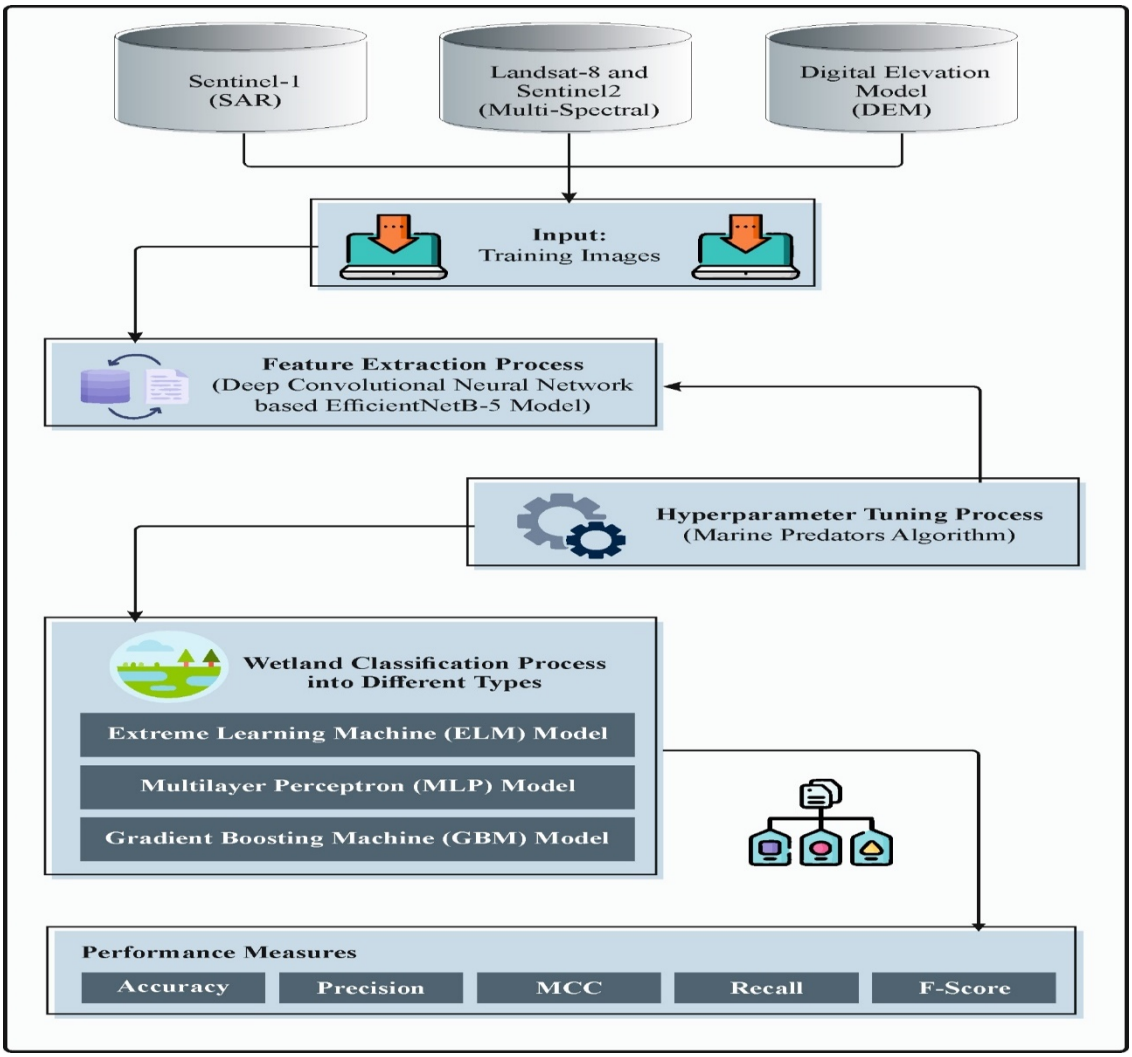

Fig. 1. Overall process of the EWC-DLFA method

3. The Proposed Method

DOI: https://doi.org/10.54216/IJAACI.060102
Received: October 29, 2023 Revised: January 20, 2023 Accepted: June 10, 2024

In this work, we have developed a new EWC-DLFA method on MS-RSI. The proposed EWC-DLFA technique examines the MS-RSI for wetland classification using the DL model which can be used for other land cover classification types. To accomplish this, the EWC-DLFA technique utilizes the data from multiple sources like Sentinel-1 (SAR), Landsat-8, Sentinel-2 (multi-spectral), and DEM. Fig. 1 illustrates the working process of the EWC-DLFA method.

3.1. Feature extractor

For the feature extractor process, the DCNN-based EfficientNetB-5 model can be applied for the extraction of features from the multi-source images. CNN is used in different kinds of problems and gained outstanding outcomes [19]. It suggestively enhanced image processing outcomes in accuracy as well as generalization. Conversely, planning the appropriate CNN design for such a problem is an important but difficult challenge. There are 3 accessible sizes for CNNs such as width, depth, and resolution. Whereas, the depth is nothing but the multiple of layers in a system. Usually, network all sizes scaling increases accurateness when equated to one or dual dimensions scaling.

Many CNN techniques are accessible with advanced outcomes in computer vision issues. EfficientNets is the most effective CNN technique. The benefits of EfficientNets is useful when compared to other most common CNNs are decreasing the number of FLOPS and parameters as well as enhancing accurateness and speed. Primary, we test with the efficient-B0 system followed by measuring all 3 sizes of this method by an effectual complex feature. Similarly, the measurement can be even, because random scaling requires tiresome physical setups and occasionally outcomes in less efficacy and accuracy.

An efficient scaling method has been projected through a compound factor to measure sizes of width, resolution, and depth. They are expressed in Eq. (1):

$$depth: d = \alpha^{\varphi}, width: w = \beta^{\varphi}, resolution: r = \gamma^{\varphi} \quad (1)$$

Where φ denotes the co-efficient defined by the consumer that manages how many resources can be accessible. Parameters of α, β, and γ define how to assign such resources to system, w, and r, individually. It was constrained $(\alpha.\beta^2.\gamma^2) \approx 2$. Normally, there are 4 scaling parameters (α, β, γ, and φ) to hunt. EfficientNets are accessible in dual phases:

Phase 1: They fix $\varphi = 1$, and then hunted optimum values for α, β, and γ measuring.

Phase 2: Giving the optimum values gained in the prior stage, fixed, β, and γ as co-efficient and created EfficientNet-B1-B7 with growing φ at 2 to 7. The MBConv block has an opposite ethereal block by a Squeeze and Excite block as well as employed in MobileNetV2. When compared to reversed ResNet, and MBConv blocks have been combined with a layer to primarily enlarge networks and then crush them.

The dissimilarity amongst the co-efficient systems is in dimensions of width, depth, and resolution. We detect in this test with EfficientNets-B0 to B4 that beneficial image data was misplaced since systems decrease image resolution. Consequently, we employ an efficient B5 framework as well as reflect the values of the parameters:

$w = 1.6,\ \alpha = 1.2,\ d = 2.2,\ r = 456,\ \gamma = 1.15\ and\ \beta = 1.1$. These parameter values are affording to the default values.

3.2. Hyperparameter tuning using MPA

The MPA-based hyperparameter tuning method is applied in order to increase the effectiveness of the EfficientNetB5 architecture. In 2020, Faramarzi et al first executed MPA. The ocean predator's behavior inspired it [20]. The MPA is a bio-inspired optimizer procedure that tracks the standards that certainly control optimal foraging approach and knowledge rate plan in aquatic surroundings.

Thus the below-mentioned are the main steps of MPA:

Beginning up the MPA: Eq. (2) shows the initial stage of the MPA, similar to that of entire population-based processes.

$$Y_0 = v + rand(l - v) \quad (2)$$

DOI: https://doi.org/10.54216/IJAACI.060102
Received: October 29, 2023 Revised: January 20, 2023 Accepted: June 10, 2024

Where y denotes the lower limit, 1 signifies the upper limit. An arbitrary vector of an array [0,1] is identified by $rand$. The Elite matrix E in Eq. (3), is created utilizing an optimal response, Y_i and has sizes with search agents (n) and total dimensions (d) is $[n, d]$.

$$E = \begin{bmatrix} y_{l,l}^{I} & y_{l_i 2}^{I} & \cdots & y_{l,d}^{I} \\ y_{2,l}^{I} & y_{2,2}^{I} & \cdots & y_{2,d}^{I} \\ \vdots & \vdots & \vdots & \vdots \\ \vdots & \vdots & \vdots & \vdots \\ \vdots & \vdots & \vdots & \vdots \\ y_{n,l}^{I} & y_{n,2}^{I} & \cdots & y_{n,d}^{I} \end{bmatrix}_{n \times d} \quad (3)$$

Eq. (4) represents that the Prey matrix P can be created by the Elite matrix's sizes.

$$P = \begin{bmatrix} Y_{1,1} & Y_{1,2} & \cdots & Y_{1,d} \\ Y_{2,1} & Y_{2,2} & \cdots & Y_{2,d} \\ \vdots & \vdots & \vdots & \vdots \\ \vdots & \vdots & \vdots & \vdots \\ \vdots & \vdots & \vdots & \vdots \\ Y_{n,1} & Y_{n,2} & \cdots & Y_{n,d} \end{bmatrix}_{n \times d} \quad (4)$$

The MPA procedure splits the rapidity gaps between the predator and its prey into 3 groups.

The predator's major excellent plan is to remain if it is quicker than the prey. At the primary 3rd round, exploration must be gradually increased A step size created employing Eq. (5) upgrades the location of the prey.

$$\overrightarrow{stepsize_\iota} = \overrightarrow{Rn_c} \otimes \left(\overrightarrow{E_\iota} - \overrightarrow{Rn_c} \otimes \overrightarrow{P_\iota}\right), i = 1,2, \ldots., n \quad (5)$$

Where Rn_c denotes the vector of random amounts. Eq. (5) determines how to upgrade the novel prey location.

$$\overrightarrow{P_\iota} = \overrightarrow{P_\iota} + 0.5.\vec{N} \otimes \overrightarrow{stepsize_\iota} \quad (6)$$

The vector N can be randomly preferred among [0,1].

The prey and predator vigorously follow their specific objectives when moving at a similar speed. The initial exploratory efforts concisely alter into directed exploitation efforts during the stage of the optimizer process. It is a significant phase for extraction as well as exploration aims. So, exploration and removal include a partial of the population. At this period, the prey is answerable for transferring out the exploitation, whereas the predator drives the exploration. During the optimization, the changeover from investigative to exploitation stages contains a wide exploration of the problem space, assessment of possible solution, and edition of the search dependent upon learning and fluctuating to directed determination once pre-defined performance convergence and threshold measures must be satisfied. At the time of exploitation stage, the prominence moves to promising areas for more accurate optimizer, rising efforts, and repeating among exploration and exploitation as required, with dynamic alterations for avoiding local goals. The main aim of such a tactical move is to competently meet optimum solutions. Eqs. (7) and (8) display the initial partial of the populations' novel locations, viewing help for exploitation.

$$\overrightarrow{stepsize_\iota} = \overrightarrow{Rn_L} \otimes (\overrightarrow{E_\iota} - \overrightarrow{Rn_B} \otimes \overrightarrow{P_\iota}) i = 1, \ldots n/2 \quad (7)$$

$$\overrightarrow{P_\iota} = \overrightarrow{P_\iota} + 0.5.\vec{N} \otimes \overrightarrow{stepsize_\iota} \quad (8)$$

Eqs. (9) and (10) display the studied population locations for the additional half, depending upon the vector Rn_L, which includes arbitrary numbers formed by the Levy distribution. The objective of this move is to inspire attention and cheer more investigation.

$$\overrightarrow{stepsize_\iota} = \overrightarrow{Rn_B} \otimes (\overrightarrow{Rn_B} \otimes \overrightarrow{E_\iota} - \overrightarrow{P_\iota}) i = n/2, \ldots, n \quad (9)$$

$$\overrightarrow{P_\iota} = \overrightarrow{E_\iota} + 0.5.\vec{B} \otimes \overrightarrow{stepsize_\iota} \quad (10)$$

DOI: https://doi.org/10.54216/IJAACI.060102
Received: October 29, 2023 Revised: January 20, 2023 Accepted: June 10, 2024

Eq. (11) was utilized as a denotation to originate the control parameter B.

$$B = (1 - \frac{Iter}{\text{Max}Iter})^{(2\frac{Iter}{\text{Max}Iter})} \tag{11}$$

With unbelievable speed, the predator has been outperforming its prey. Such a condition matures, the optimizer procedure could be finished efficiently and is regularly related to an important probable for exploitation. Eqs. (12) and (13) demonstrate how the positions of prey are upgraded.

$$\overrightarrow{stepsize_i} = \overrightarrow{Rn_L} \otimes (\overrightarrow{Rn_L} \otimes \overrightarrow{E_i} - \overrightarrow{P_i}) i = 1, \ldots, n \tag{12}$$

$$\overrightarrow{P_i} = \overrightarrow{E_i} + 0.5.\vec{B} \otimes \overrightarrow{stepsize_i} \tag{13}$$

Fish Aggregating Devices (FAD) have been developed in order to remain the search. Eq. (14), a representation of FAD is expressed as below:

$$\overrightarrow{P_l} = \begin{cases} \overrightarrow{P_i} + CF[Y_{\min} + \overrightarrow{Rn} \otimes (\overline{Y}_{\max} - \overline{Y}_{\min})] \otimes \vec{V} \\ if\ rn \leq FADs \\ \overrightarrow{P_l} + [FADs(1-rn) + rn](\overline{p1} - \overline{p_{r2}}) \\ if\ rn > FADs \end{cases} \tag{14}$$

The fitness selection has been a significant factor prompting the effectiveness of the MPA method. The hyperparameter selection technique includes the solution encoding algorithm for measuring the efficacy of candidate solutions. Now, the MPA method deliberates accuracy as the main condition to determine the fitness function (FF) to be developed as given below.

$$Fitness = \max(P) \tag{15}$$

$$P = \frac{TP}{TP + FP} \tag{16}$$

From the mathematical formula, FP describes the false positive value and TP denotes the true positive.

3.3. Ensemble Classification

In this work, an ensemble of three ML classifiers such as ELM, MLP, and GBM are used to classify the wetland into different types such as fen, bog, marsh, swamps, and upland.

3.3.1. ELM Model

The ELM is a classical SLFN. The ELM is not required to modify parameters through rounds and does not have the features of a slower speed of training in contrast to other SLFNs [21]. The least-square model determines the weights for the β output layer while the weights W and biases B are randomly allocated. Consider the hidden layer (HL) of ELM has n nodes. The ELM could choose some non-linear, piecewise continual excitation function (x). The output matrix T and the output of HL is formulated by the following expression:

$$H = g(WX + B) \tag{17}$$

$$T' = H\beta \tag{18}$$

The loss function E is formulated by:

$$E = \min_{\beta} ||H\beta - y|| \tag{19}$$

Then, β is computed as follows:

$$\beta = H^{+}Y' \tag{20}$$

DOI: https://doi.org/10.54216/IJAACI.060102
Received: October 29, 2023 Revised: January 20, 2023 Accepted: June 10, 2024

In Eq. (13), the MP-generalized inverse matrix of H is represented as H^{+}. The least-square solution with a decreased model can be attained by the MP-generalized inverse matrix, making the ELM will be better generalization performance and robustness.

3.3.2. MLP Model

FNN is the most prevalent type of NN architecture, which could be noticed and predicted by computational methods by applying innovative parallel layer architecture [22]. The MLP has a form of the FNNs, which is implemented in various domains in the research. It is exposed for learning generalized internal images of intricate non-linear mappings. The MLP includes numerous layers. A primary layer can be named the input layer in which final layer is termed as output layer, and the middle layers are known as the hidden layers (HL). The nodes have differed under the count of hidden neurons and v inputs, which execute 2 functions, such as activation and summation. The weighted total of the inputs can be measured by Eq. (21).

$$Sum_j = \sum_{i=1}^{n} w_{i,j}\, I_i + \beta_j \tag{21}.$$

where w_{ij} describes the link weight of the i^{th} nodes at the input layer as well as the jth nodes at HL, n refers to the number of input nodes, β_j describes bias values in j^{th} hidden nodes, and I_i represents the ith input. The activation method has been introduced by employing the values attained from the formula. Numerous activation processes have been applied in MLPs. The major extensive implementation of this can be the sigmoid function as well as its mathematical formula as given in Eq. (22).

$$f_j(x) = \frac{1}{1 + e^{-Sum_j}} \tag{22}$$

Thus, in the HL, the output of all neurons could be determined; the last output of the network must be measured in Eq. (23).

$$y_i = f_j\left(\sum_{i=1}^{n} w_{i,j}\, I_i + \beta_j\right) \tag{23}$$

As per presented in the formula, the bias and weight values promptly impact the MLP features. For determining the higher effectiveness among the inputs and outputs, bias and weight values are required for capturing optimum values. Fig. 2 depicts the infrastructure of MLP.

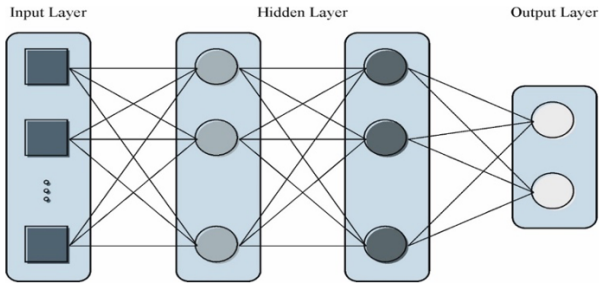

Fig. 2. Architecture of MLP

3.3.3. GBM Model

GBM integrates a group of weaker learners by considering the resultant error at round till a stronger learner has been attained as the addition of consecutive weaker ones [23].

DOI: https://doi.org/10.54216/IJAACI.060102
Received: October 29, 2023 Revised: January 20, 2023 Accepted: June 10, 2024

Consider $D = \{x_n, y_n\}_{n=1}^{N}$ as a training example where the gradient boosting can be determined as an optimum approximation $F(x)$ of $F^*(x)$ function, mapping the instance x_n to y_n to reduce the expected values of loss function $L\big(y, F(x)\big)$ over the dissemination of each training example.

$$F^*(x) = \text{argmin}_{F(x)} L_{x,y}\big(y, F(x)\big) \tag{24}$$

GBM exploits a logistic loss function for the classification to approximate $L\big(y, F(x)\big) = \big(y - F(x)\big)$. GBM begins with weaker learner $F(x)$ is a constant value and fits weaker learner to precise the error generated through the prior weaker learner to reinforce the predictive accuracy by minimalizing loss function over the boosting phase. At every phase, the local minimal proportion takes a step for the loss function negative gradient to determine the local minima. The gradient direction of loss function in i^{th} boosting phase is evaluated as follows:

$$r_{i,n} = -\left[\frac{\partial L\big(y_n, F(x_n)\big)}{\partial F(x_n)}\right]_{F(x)=F_{i-1}(x)} \tag{25}$$

GBM is used to generalize the computation range of gradient once the regression tree is utilized with a parameter as a weaker learner, generally, a parameter function of input variable x, considered by the parameter and ∂ shows the partial derivative. A tree could be attained by resolving the subsequent expression:

$$a_i = \text{argmin}_{a,\beta} \sum_{n=1}^{N} \big[r_{i,n} - \beta h(x_n, a)\big]^2 \tag{26}$$

In Eq. (26), the parameter a_i is attained at i^{th} iterations and the weight values is β. The optimum length p_i is defined, and $F_i(x)$ model is updated at i^{th} iterations, with $t = 1$ to T amount of iterations.

The choice of base learner and loss function derived in the GBM facilitates further development and design by the researcher workers dependent upon the task requirement. It goal is to create classification mechanisms for the CP application by improving the architecture of the GBM and its hyperparameters.

4. Performance Validation

The wetland classification performance of the EWC-DLFA technique can be examined using multi-source remote sensing image data. It comprises 1250 samples with five classes as demonstrated in Table 1.

Table 1: Details on dataset

Class	**No. of Samples**
Fen	250
Bog	250
Marsh	250
Swamp	250
Upland	250
Total Samples	**1250**

Fig. 3 exhibits the confusion matrices accomplished by the EWC-DLFA method with 80:20 TRPH/TSPH and 70% of TRPH:30%TSPH. The obtained findings demonstrate the efficient recognition with five classes.

DOI: https://doi.org/10.54216/IJAACI.060102
Received: October 29, 2023 Revised: January 20, 2023 Accepted: June 10, 2024

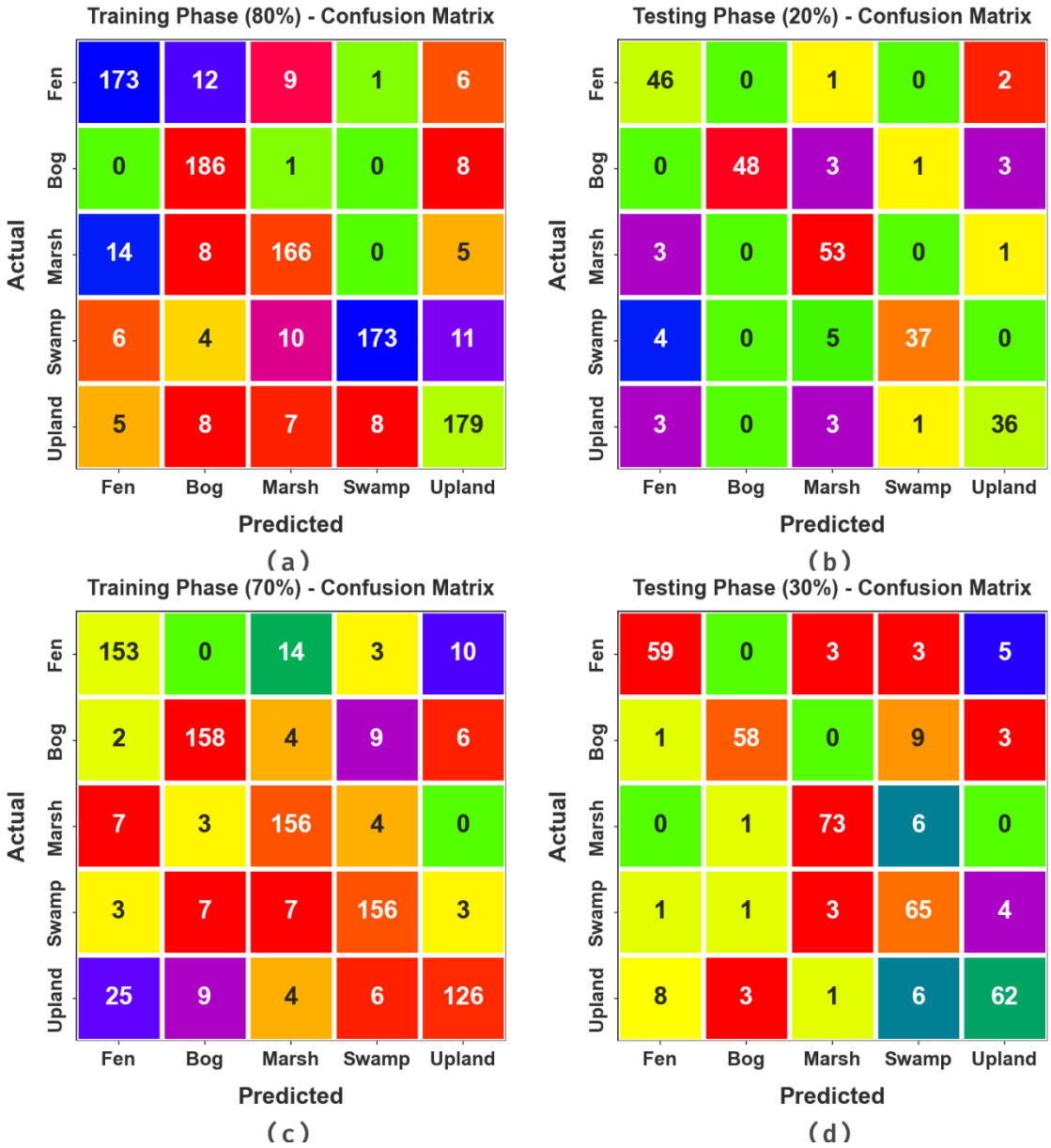

Fig. 3. Confusion matrices of EWC-DLFA model (a-b) 80%ofTRPH:20%ofTSPH and (c-d) 70% of TRPH:30% ofTSPH

The wetland classification outcomes of the EWC-DLFA method on 80%ofTRPH:20%ofTSPH is represented in Table 2 and Fig. 4. The experimental findings display the EWC-DLFA technique appropriately categorizes the wetland classes. On 80% of TRPH, the EWC-DLFA method gains average $accu_y$ of 95.08%, $prec_n$ of 87.88%, $reca_l$ of 87.75%, F_{score} of 87.70% and MCC of 84.71%. Simultaneously, with 20% of TSPH, the EWC-DLFA methodology gets average $accu_y$ of 95.20%, $prec_n$ of 88.85%, $reca_l$ of 87.66%, F_{score} of 87.89% and MCC of 85.17%.

Table 2: Wetland classification outcome of EWC-DLFA model under 80%ofTRPH:20%ofTSPH

Classes	$Accu_y$	$Prec_n$	$Reca_l$	F_{score}	MCC
TRPH (80%)					
Fen	94.70	87.37	86.07	86.72	83.41
Bog	95.90	85.32	95.38	90.07	87.72
Marsh	94.60	86.01	86.01	86.01	82.66
Swamp	96.00	95.05	84.80	89.64	87.39

DOI: https://doi.org/10.54216/IJAACI.060102
Received: October 29, 2023 Revised: January 20, 2023 Accepted: June 10, 2024

Upland	94.20	85.65	86.47	86.06	82.40
Average	**95.08**	**87.88**	**87.75**	**87.70**	**84.71**
TSPH (20%)					
Fen	94.80	82.14	93.88	87.62	84.65
Bog	97.20	100.00	87.27	93.20	91.79
Marsh	93.60	81.54	92.98	86.89	82.99
Swamp	95.60	94.87	80.43	87.06	84.85
Upland	94.80	85.71	83.72	84.71	81.58
Average	**95.20**	**88.85**	**87.66**	**87.89**	**85.17**

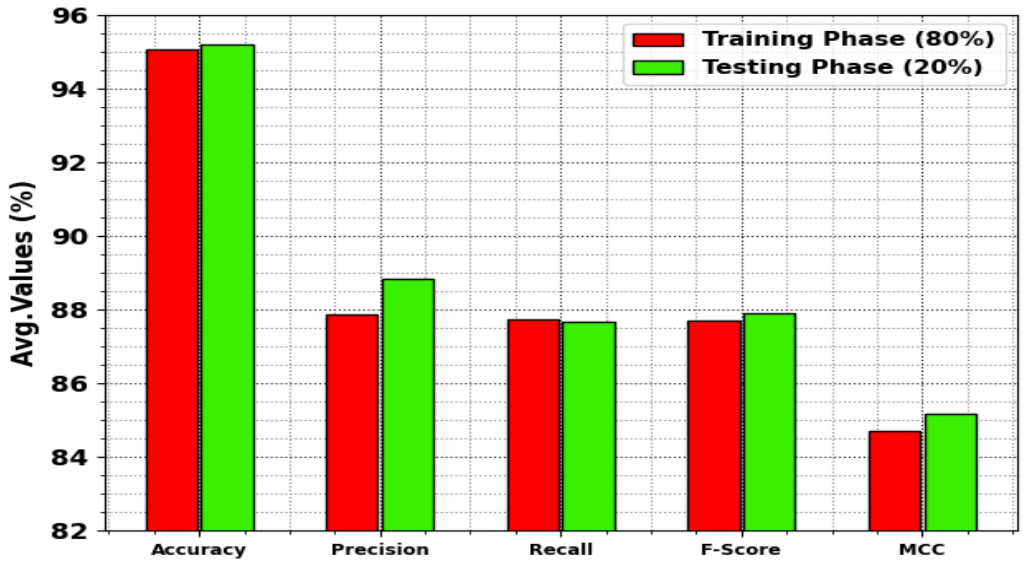

Fig. 4. Average outcome of the EWC-DLFA model with 80%ofTRPH:20%ofTSPH

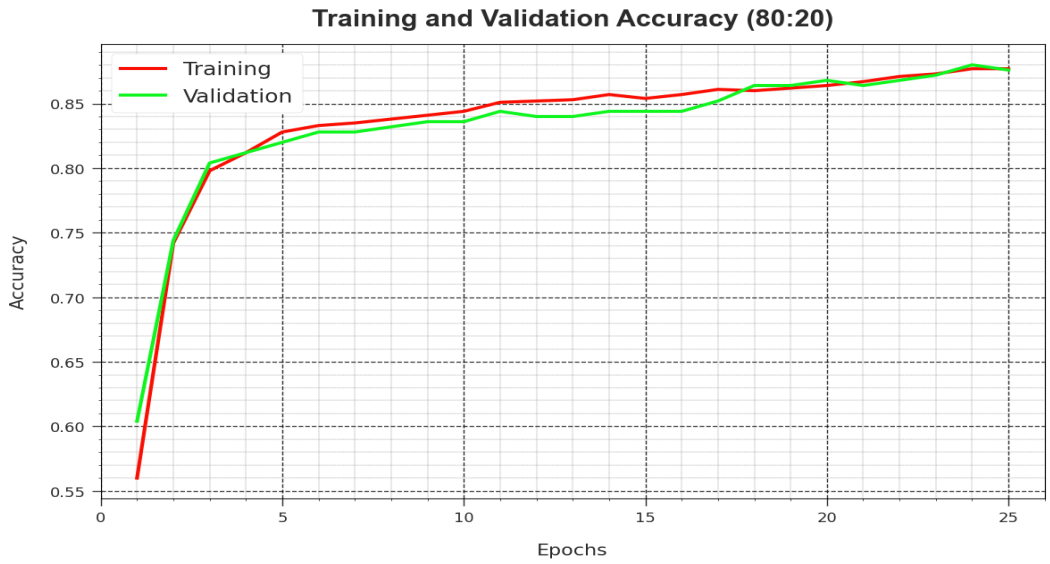

Fig. 5. $Accu_y$ curve of the EWC-DLFA system under 80%ofTRPH:20%ofTSPH

DOI: https://doi.org/10.54216/IJAACI.060102
Received: October 29, 2023 Revised: January 20, 2023 Accepted: June 10, 2024

The $accu_y$ curves for training (TR) and validation (VL) displays in Fig. 5 for the EWC-DLFA method on 80%ofTRPH:20%ofTSPH provides clear understanding into its effectiveness at different epochs. Particularly, it becomes a constant upgrading in the TR and TS $accu_y$ with increased epochs, indicating the model's ability at learning and identifying patterns on both dataset. The upward tendency in TS $accu_y$ underscores the adaptability of model for the dataset of TR as well as its abilities to generate accurate predictions on unobserved dataset, emphasizing capabilities of strong generalization.

Fig. 6 provides a detailed review of the TR and TS loss values for the EWC-DLFA method on 80%ofTRPH:20%ofTSPH across various epochs. The TR loss consistently decreases as the model refines its weights to decrease classifier errors on both datasets. The loss curves clearly illustrate the model's alignment with the TR dataset, emphasizing its ability to capture patterns effectively in both datasets. Notable is the continuous refinement of parameter in the EWC-DLFA system, aimed at minimizing discrepancies between predictions and actual TR labels.

Fig. 6. Loss curve of the EWC-DLFA method with 80%ofTRPH:20%ofTSPH

The wetland classification analysis of the EWC-DLFA methodology on 70%of TRPH:30%TSPH can be exhibited in Table 3 and Fig. 7. The accomplished values demonstrate the EWC-DLFA method correctly categorizes the wetland classes. According to 70% of TRPH, the EWC-DLFA system provides average $accu_y$ of 94.24%, $prec_n$ of 85.73%, $reca_l$ of 85.56%, F_{score} of 85.50% and MCC of 82.01%. Simultaneously, based on 30% of TSPH, the EWC-DLFA methodology obtains average $accu_y$ of 93.81%, $prec_n$ of 85.13%, $reca_l$ of 84.51%, F_{score} of 84.60% and MCC of 80.90%.

Table 3: Wetland classification analysis of EWC-DLFA model with 70%of TRPH:30%TSPH

Classes	$Accu_y$	$Prec_n$	$Reca_l$	F_{score}	MCC
TRPH (70%)					
Fen	92.69	80.53	85.00	82.70	78.12
Bog	95.43	89.27	88.27	88.76	85.90
Marsh	95.09	84.32	91.76	87.89	84.93
Swamp	95.20	87.64	88.64	88.14	85.13
Upland	92.80	86.90	74.12	80.00	76.00
Average	**94.24**	**85.73**	**85.56**	**85.50**	**82.01**
TSPH (30%)					
Fen	94.40	85.51	84.29	84.89	81.46
Bog	95.20	92.06	81.69	86.57	83.88
Marsh	96.27	91.25	91.25	91.25	88.88
Swamp	91.20	73.03	87.84	79.75	74.71
Upland	92.00	83.78	77.50	80.52	75.59
Average	**93.81**	**85.13**	**84.51**	**84.60**	**80.90**

DOI: https://doi.org/10.54216/IJAACI.060102
Received: October 29, 2023 Revised: January 20, 2023 Accepted: June 10, 2024

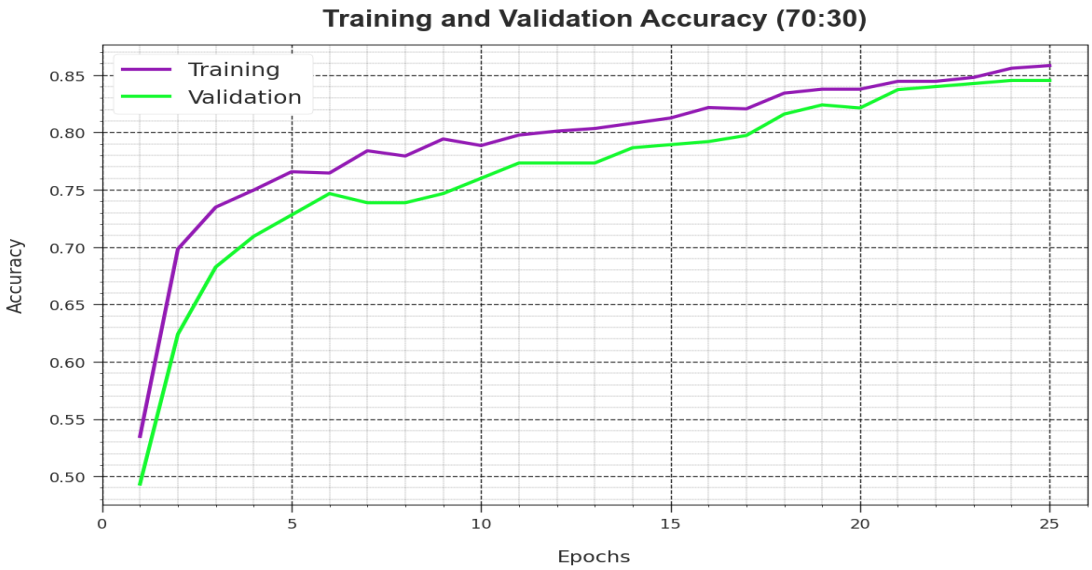

Fig. 7. Average outcome of the EWC-DLFA approach on 70%of TRPH:30%TSPH

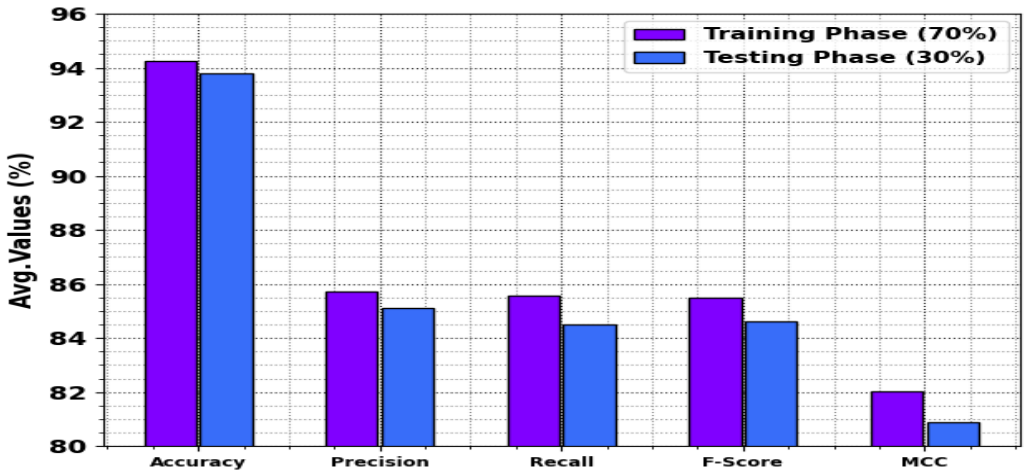

Fig. 8. $Accu_y$ curve of the EWC-DLFA method at 70%of TRPH:30%TSPH

The $accu_y$ curves for training (TR) and validation (VL) demonstrated in Fig. 8 for the EWC-DLFA algorithm at 70%of TRPH:30%TSPH offer respected insights into its efficiency in varied epochs. Especially, there is a reliable development in both TR and TS $accu_y$ with improving epochs, specifying the model's proficiency in learning and identifying patterns in TR and TS datasets. The increasing tendency in TS $accu_y$ underscores the adaptability of the model to the TR dataset and abilities for creating correct predictions on hidden dataset, emphasizing strong generalisabilities.

Fig. 9 displays a comprehensive review of the TR and TS loss values for the EWC-DLFA approach on 70%of TRPH:30%TSPH through different epochs. The TR loss dependably diminutions as the model refines its weights for decreasing classifier error rates on these datasets. The loss curves represent the model's configuration with the TR dataset, underscoring its ability for efficiently capturing patterns efficiently. Noteworthy can be the constant improvement of parameters in the EWC-DLFA algorithm, targets at minimalizing discrepancies amongst predictions and actual TR labels.

DOI: https://doi.org/10.54216/IJAACI.060102
Received: October 29, 2023 Revised: January 20, 2023 Accepted: June 10, 2024

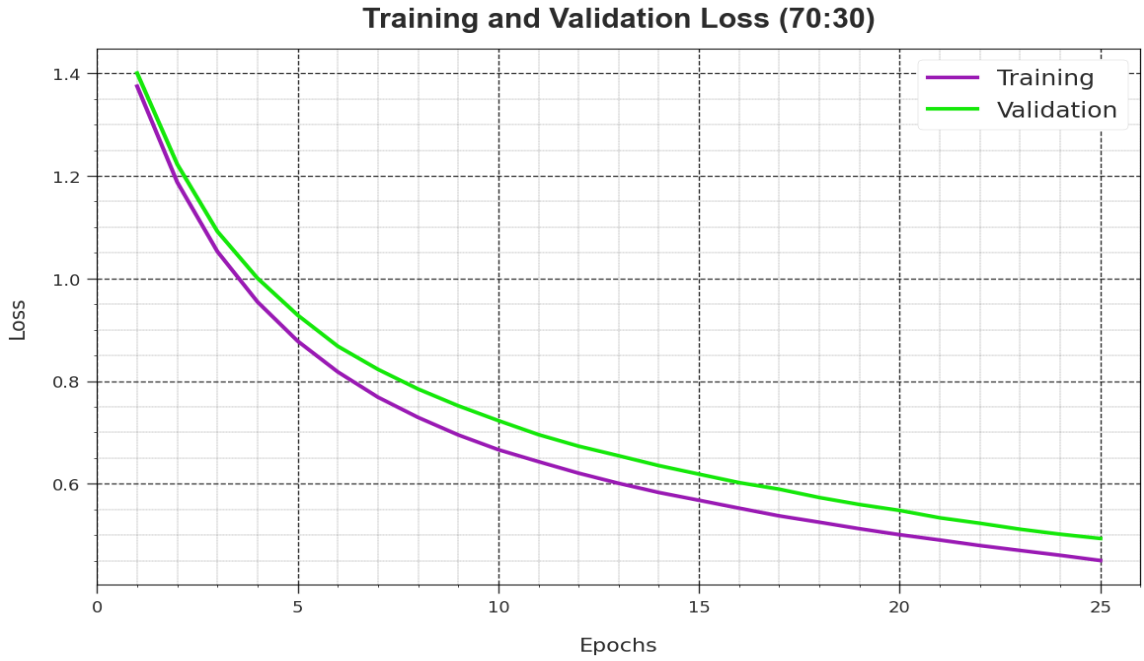

Fig. 9. Loss curve of the EWC-DLFA method with 70%of TRPH:30%TSPH

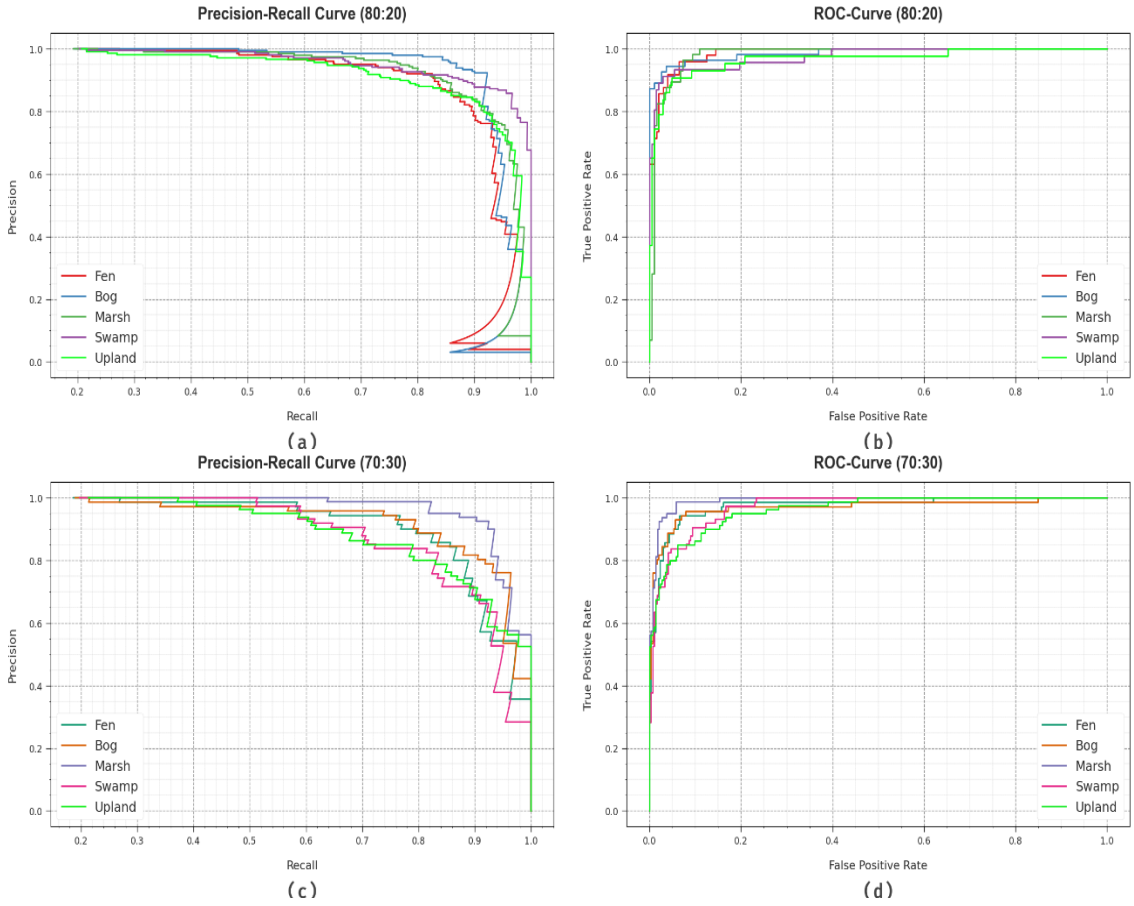

Fig. 10. (a-c) PR curve on 80:20 and 70:30 and (b-d) ROC curve on 80:20 and 70:30

DOI: https://doi.org/10.54216/IJAACI.060102
Received: October 29, 2023 Revised: January 20, 2023 Accepted: June 10, 2024

Fig. 10 displays the classifier analysis of the EWC-DLFA system at 80:20 and 70:30. Figs. 10a-10c represents the PR effectiveness of the EWC-DLFA technique. The achieved outcomes show the EWC-DLFA algorithm gains improving values of PR. Moreover, it could be noticeable that the EWC-DLFA system gets higher PR values with five classes. Also, Figs. 10b-10d exhibits the ROC analysis of the EWC-DLFA technique. This figure denotes the EWC-DLFA algorithm acquires boosted ROC values. Also, the EWC-DLFA system offers increased ROC values with five classes.

The comparison analysis of the EWC-DLFA technique is provided with existing models in Table 4 and Fig. 11 [24]. The achieved outcome showcases that the VGG-16 and DenseNet models offer worse performance whereas the AlexNet and Inception-v3 models obtain closer performance. Meanwhile, VGG-19 and ResNet-50 models accomplish near-optimal results. However, the EWC-DLFA technique reaches better performance over other models with maximum $accu_y$ of 95.20%, $prec_n$ of 88.85%, $reca_l$ of 87.66%, and F_{score} of 87.89% respectively.

Table 4: Comparison analysis of the EWC-DLFA methodology with other techniques

Classifiers	$Accu_y$	$Prec_n$	$Reca_l$	F_{score}
EWC-DLFA	95.20	88.85	87.66	87.89
AlexNet	92.79	75.00	70.44	85.73
VGG16	89.28	81.82	72.74	85.60
VGG19	94.79	86.07	84.28	74.16
InceptionV3	91.65	69.35	85.01	69.14
DenseNet	89.73	79.15	79.71	81.65
ResNet50	93.18	86.90	82.83	83.75

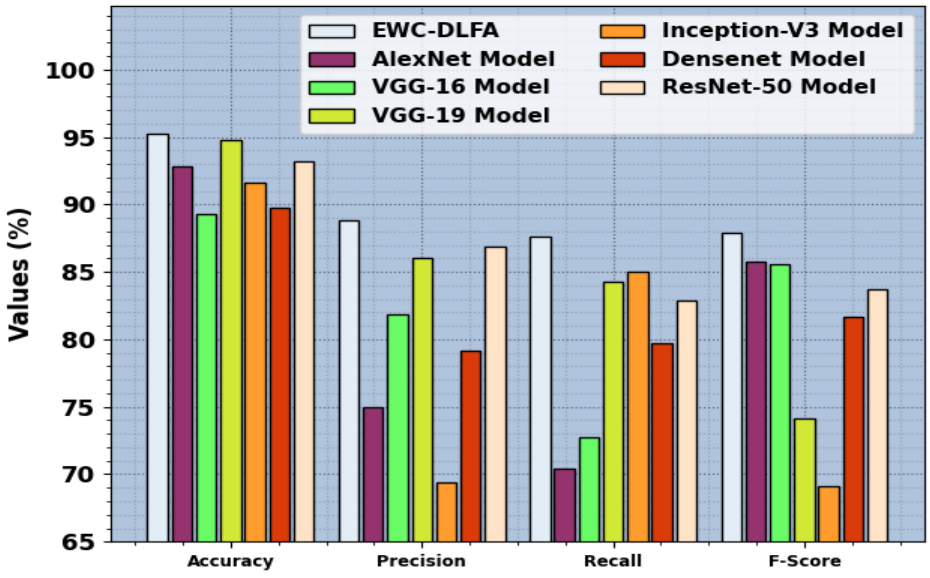

Fig. 11. Comparison analysis of the EWC-DLFA algorithm with other system

The computation time (CT) analysis of the EWC-DLFA technique is compared with recent approaches provided in Table 5 and Fig. 12. The achieved findings depict that the EWC-DLFA technique reaches the least CT of 0.85s. On the other hand, the AlexNet, VGG16, VGG19, Inception-v3, DenseNet, and ResNet50 models obtain increased CT values of 2.98s, 2.45s, 1.86s, 2.30s, 1.80s, and 1.91s, correspondingly. Therefore, the EWC-DLFA technique can be utilized for enhanced performance over other compared models.

DOI: https://doi.org/10.54216/IJAACI.060102
Received: October 29, 2023 Revised: January 20, 2023 Accepted: June 10, 2024

Table 5: CT analysis of the EWC-DLFA model with other methodologies

Classifiers	Computational Time (sec)
EWC-DLFA	0.85
AlexNet	2.98
VGG16	2.45
VGG19	1.86
InceptionV3	2.30
DenseNet	1.80
ResNet50	1.91

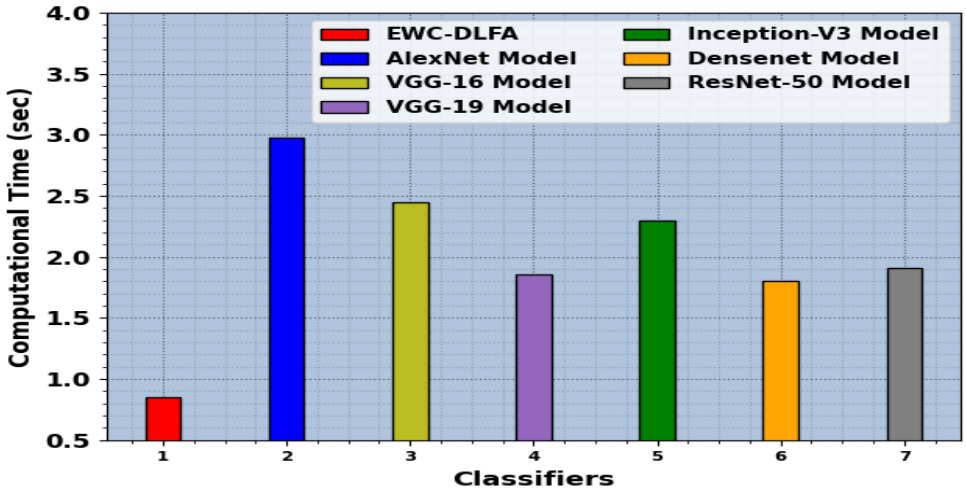

Fig. 12. CT analysis of the EWC-DLFA method with other algorithms

5. Conclusion

In this article, we have designed an innovative EWC-DLFA technique on MS-RSI. The proposed EWC-DLFA technique examines the MS-RSI for wetland classification using the DL model which can be used for other land cover classification types. To accomplish this, the EWC-DLFA technique utilizes the data from multiple sources such as Sentinel-1 (SAR), Landsat-8 and Sentinel-2 (multi-spectral), and DEM. In the presented EWC-DLFA technique, a deep convolutional neural network-based EfficientNetB-5 model can be applied for the extraction of features from multi-source images. For increasing the performance of the EfficientNet-B5 architecture, the MPA-based hyper parameter tuning process can be applied. Finally, an ensemble of three ML classifiers such as ELM, MLP, and GBM are used to classify the wetland into different types such as fen, bog, marsh, swamps, and upland. The performance of the EWC-DLFA technique can be validated using a large set of simulations. The resultant values pointed out that the EWC-DLFA technique reaches better performance over other models on wetland classification.

References

[1] Ahmed, K.R.; Akter, S.; Marandi, A.; Schüth, C. A Simple and Robust Wetland Classification Approach by Using Optical Indices, Unsupervised and Supervised Machine Learning Algorithms. Remote Sens. Appl. Soc. Environ. 2021, 23, 100569.

[2] Miyamoto, M.; Kushida, K.; Yoshino, K.; Nagano, T.; Sato, Y. Evaluation of multispatial scale measurements for monitoring wetland vegetation, Kushiro wetland, JAPAN: Application of SPOT images, CASI data, airborne CNIR video images and balloon aerial photography. In Proceedings of the

DOI: https://doi.org/10.54216/IJAACI.060102
Received: October 29, 2023 Revised: January 20, 2023 Accepted: June 10, 2024

IGARSS 2003: IEEE International Geoscience and Remote Sensing Symposium, Learning from Earth's Shapes and Sizes, Toulouse, France, 21–25 July 2003; Volume I–VII, pp. 3275–3277.

[3] van Asselen, S.; Verburg, P.H.; Vermaat, J.E.; Janse, J.H. Drivers of Wetland Conversion: A Global Meta-Analysis. PLoS ONE 2013, 8, e81292.

[4] Mahdianpari, M.; Brisco, B.; Granger, J.; Mohammadimanesh, F.; Salehi, B.; Homayouni, S.; Bourgeau-Chavez, L. The Third Generation of Pan-Canadian Wetland Map at 10 m Resolution Using Multisource Earth Observation Data on Cloud Computing Platform. IEEE J. Sel. Top. Appl. Earth Obs. Remote Sens. 2021, 14, 8789–8803.

[5] Amani, M.; Mahdavi, S.; Afshar, M.; Brisco, B.; Huang, W.; Mirzadeh, S.M.J.; White, L.; Banks, S.; Montgomery, J.; Hopkinson, C. Canadian Wetland Inventory using Google Earth Engine: The First Map and Preliminary Results. Remote Sens. 2019, 11, 842.

[6] Bwangoy, J.-R.B.; Hansen, M.C.; Roy, D.P.; De Grandi, G.; Justice, C.O. Wetland mapping in the Congo Basin using optical and radar remotely sensed data and derived topographical indices. Remote Sens. Environ. 2010, 114, 73–86.

[7] Ceron, C.N.; Melesse, A.M.; Price, R.; Dessu, S.B.; Kandel, H.P. Operational actual wetland evapotranspiration estimation for South Florida using MODIS imagery. Remote Sens. 2015, 7, 3613–3632.

[8] Davranche, A.; Lefebvre, G.; Poulin, B. Wetland monitoring using classification trees and SPOT-5 seasonal time series. Remote Sens. Environ. 2010, 114, 552–562.

[9] Mahdianpari, M.; Salehi, B.; Mohammadimanesh, F.; Motagh, M. Random forest wetland classification using ALOS-2 L-band, RADARSAT-2 C-band, and TerraSAR-X imagery. ISPRS J. Photogramm. Remote Sens. 2017, 130, 13–31.

[10] Shafizadeh-Moghadam, H.; Khazaei, M.; Alavipanah, S.K.; Weng, Q. Google Earth Engine for Large-Scale Land Use and Land Cover Mapping: An Object-Based Classification Approach Using Spectral, Textural and Topographical Factors. GIScience Remote Sens. 2021, 58, 914–928.

[11] Jamali, A., Mahdianpari, M., Brisco, B., Mao, D., Salehi, B. and Mohammadimanesh, F., 2022. 3DUNetGSFormer: A deep learning pipeline for complex wetland mapping using generative adversarial networks and Swin transformer. *Ecological Informatics*, *72*, p.101904.

[12] Hosseiny, B., Mahdianpari, M., Brisco, B., Mohammadimanesh, F. and Salehi, B., 2021. WetNet: A spatial–temporal ensemble deep learning model for wetland classification using Sentinel-1 and Sentinel-2. *IEEE Transactions on Geoscience and Remote Sensing*, *60*, pp.1-14.

[13] Guo, F., Li, Z., Meng, Q., Ren, G., Wang, L., Wang, J., Qin, H. and Zhang, J., 2023. Semi-supervised cross-domain feature fusion classification network for coastal wetland classification with hyperspectral and LiDAR data. *International Journal of Applied Earth Observation and Geoinformation*, *120*, p.103354.

[14] Zhao, J., Wang, L., Yang, H., Wu, P., Wang, B., Pan, C. and Wu, Y., 2022. A land cover classification method for high-resolution remote sensing images based on NDVI deep learning fusion network. *Remote Sensing*, *14*(21), p.5455.

[15] Bosco, M.J., Wang, G. and Hategekimana, Y., 2021. Learning multi-granularity neural network encoding image classification using DCNNs for Easter Africa Community Countries. *IEEE Access*, *9*, pp.146703-146718.

[16] Hu, X., Zhang, P., Zhang, Q. and Wang, J., 2021. Improving wetland cover classification using artificial neural networks with ensemble techniques. *GIScience & Remote Sensing*, *58*(4), pp.603-623.

[17] Yan, J., Liu, J., Liang, D., Wang, Y., Li, J. and Wang, L., 2023. Semantic segmentation of land cover in urban areas by fusing multi-source satellite image time series. *IEEE Transactions on Geoscience and Remote Sensing*.

[18] Jafarzadeh, H., Mahdianpari, M. and Gill, E.W., 2022. Wet-GC: A Novel Multimodel Graph Convolutional Approach for Wetland Classification Using Sentinel-1 and 2 Imagery with Limited Training Samples. *IEEE Journal of Selected Topics in Applied Earth Observations and Remote Sensing*, *15*, pp.5303-5316.

[19] Pour, A.M., Seyedarabi, H., Jahromi, S.H.A. and Javadzadeh, A., 2020. Automatic detection and monitoring of diabetic retinopathy using efficient convolutional neural networks and contrast limited adaptive histogram equalization. *IEEE Access*, *8*, pp.136668-136673.

[20] Sekhar, J.C., Rajyalakshmi, C., Nagaraj, S., Sankar, S., Saturi, R. and Harshavardhan, A., 2023. Deep Generative Adversarial Networks with Marine Predators Algorithm for Classification of Alzheimer's Disease Using Electroencephalogram. *Journal of King Saud University-Computer and Information Sciences*, p.101848.

DOI: https://doi.org/10.54216/IJAACI.060102
Received: October 29, 2023 Revised: January 20, 2023 Accepted: June 10, 2024

[21] Xiao, D., Li, B., Shan, J., Yan, Z. and Huang, J., 2023. SOC Estimation of Vanadium Redox Flow Batteries Based on the ISCSO-ELM Algorithm. *ACS Omega*.
[22] Altay, O. and Varol Altay, E., 2023. A novel hybrid multilayer perceptron neural network with improved grey wolf optimizer. *Neural Computing and Applications*, *35*(1), pp.529-556.
[23] AlShourbaji, I., Helian, N., Sun, Y., Hussien, A.G., Abualigah, L. and Elnaim, B., 2023. An efficient churn prediction model using gradient boosting machine and metaheuristic optimization. *Scientific Reports*, *13*(1), p.14441.
[24] Judah, A. and Hu, B., 2022. An advanced data fusion method to improve wetland classification using multi-source remotely sensed data. *Sensors*, *22*(22), p.8942.

DOI: https://doi.org/10.54216/IJAACI.060102
Received: October 29, 2023 Revised: January 20, 2023 Accepted: June 10, 2024